Scripta Materialia 139 (2017) 96–99

Contents lists available at ScienceDirect

Scripta Materialia

journal homepage: www.elsevier.com/locate/scriptamat

Regular article

Influence of powder properties on densification mechanism during spark plasma sintering

C. Yang [a,*], M.D. Zhu [a], X. Luo [a], L.H. Liu [b], W.W. Zhang [a], Y. Long [a], Z.Y. Xiao [a], Z.Q. Fu [a,d], L.C. Zhang [a,c], E.J. Lavernia [d,*]

[a] National Engineering Research Center of Near-net-shape Forming for Metallic Materials, South China University of Technology, Guangzhou 510640, China
[b] Department of Mechanical Engineering, Tsinghua University, Beijing 100084, China
[c] School of Engineering, Edith Cowan University, 270 Joondalup Drive, Joondalup, Perth, WA 6027, Australia
[d] Department of Chemical Engineering and Materials Science, University of California, Irvine, CA 92697, USA

ARTICLE INFO

Article history:
Received 8 February 2017
Received in revised form 6 June 2017
Accepted 18 June 2017
Available online xxxx

Keywords:
Titanium alloys
Powder consolidation
Spark plasma sintering
Mechanical milling

ABSTRACT

We report on the formulation of a factor, *f*, that when applied together with the activation energy for viscous flow (*Q*), can be used to provide important insight into the densification mechanism that are active during powder sintering. We ascertain the validity of this formulation by comparing the densification behaviour of atomized and milled powders for Ti-6Al-4V alloy and pure Ti during spark plasma sintering, and identifying the underlying mechanisms.

Powder sintering is widely used to manufacture high performance, bulk metals and alloys of various compositions [1–5]. In general, the powder particles that are used during sintering can be classified in terms of their geometry: spherical powders, which are generally synthesized using atomization, and irregular powders, which can be prepared using chemical or mechanical methods, such as precipitation and milling, respectively. For a given composition, spherical and irregular powders will differ in terms of various physical parameters [6], such as surface energy (γ), average particle size (D), viscosity (η), etc. In general, the value of γ increases as D decreases, and is higher for an irregular geometry; similarly, both fluidity and apparent density increase with increasing D and a more regular geometry. It then follows that powder morphology will influence the electrical, mass and thermal transport fields during powder sintering, and therefore the underlying densification mechanisms [1–2]. This is evidenced by published studies which show that a high value of γ, in combination with smaller values of D, and η will accelerate powder shrinkage and densification [7–11]. However, it is difficult to isolate the influence of a single physical parameter on densification, given the interrelationships between γ, D, η and geometry.

From the above discussion, it would be helpful to identify a factor, defined hereafter as *f*, which in combination with the activation energy for viscous flow (Q), can be used to provide insight into the underlying densification mechanisms. In essence, the values of *f* and *Q* are related to the properties of the as-sintered bulk alloys, such as porosity and/or relative density, and therefore will affect mechanical behavior. Notably, this represents the first attempt to establish a framework that can be used to determine the value of an index *f*.

We illustrate the validity of the proposed framework by considering atomized spherical and milled irregular powders examples for Ti-6Al-4V alloy and pure Ti. Interestingly, as will be demonstrated below, the values for the as-derived *f* and *Q* for the spherical powders are always greater than the corresponding ones of the irregular powders.

During powder sintering, the instantaneous relative density ρ (%) of the sintered compact can be calculated as [7]:

$$\rho = \frac{L_0}{L}\rho_0 \tag{1}$$

where ρ_0 (%) is the initial relative density, L_0 (mm) the initial height of the powders in the die, and L (mm) the height when specimen reaches the relative density of ρ. The instantaneous densification rate $\dot{\rho}$ (s^{-1}) is then estimated by [7]:

$$\dot{\rho} = \frac{d\rho_i}{dt_i} = \frac{\rho_i - \rho_{i-1}}{t_i - t_{i-1}} \tag{2}$$

where ρ_i (%) is the instantaneous relative density at time t_i (s), and the time interval (t_i-t_{i-1}) is 1 s.

* Corresponding authors.
E-mail addresses: cyang@scut.edu.cn (C. Yang), lavernia@uci.edu (E.J. Lavernia).

http://dx.doi.org/10.1016/j.scriptamat.2017.06.034
1359-6462/

On the basis of the Frenkel model used for Newtonian viscous materials [12], the densification behavior of powder particles under isothermal conditions is determined by the physical properties of the powder, expressed by:

$$\frac{\Delta L}{L_0} = \frac{3\gamma}{4D\eta}t \tag{3}$$

where $\Delta L/L_0$ is the shrinkage of the powder, γ (J/m^2) the surface energy, t (s) the time, D (m) the average particle size, and η (Pa·s) the viscosity of the powder materials.

Over a limited temperature range, η is temperature dependent and follows an Arrhenius relationship [13]:

$$\eta = \eta_0 \exp\left(\frac{Q}{RT}\right) \tag{4}$$

where η_0 (Pa·s) is the frequency factor, Q the activation energy for viscous flow, R (8.314 J/K/mol) the universal gas constant, and T (K) the absolute temperature. The relationship between T and time t in an isochronal experiment can be expressed as:

$$\frac{dT}{dt} = c \tag{5}$$

where c (K/s) is heating rate. Hence, by differentiating Eq. (3) with respect to T and applying Eqs. (4) and (5), the shrinkage rate under isochronal heating conditions may be estimated as:

$$\frac{d\left(\frac{\Delta L}{L_0}\right)}{dT} = \frac{3\gamma}{4Dc\eta_0}\exp\left(\frac{-Q}{RT}\right) \tag{6}$$

Taking the logarithm of both sides, Eq. (6) is written as:

$$\ln\left(\frac{d\left(\frac{\Delta L}{L_0}\right)}{dT}\right) = \ln\left(\frac{3\gamma}{4Dc\eta_0}\right) - \frac{Q}{RT} \tag{7}$$

In general, for a given composition, γ, D and η_0 remain constant. In our case, therefore, we introduce a factor f defined in terms of these physical properties:

$$f = \frac{3\gamma}{4D\eta_0} \tag{8}$$

As such, the factor f and the activation energy Q for a particular heating rate can be determined from the slope and the intercept respectively from plots of $\ln(d(\Delta L / L_0) / dT)$ versus $1/T$ (Eq. (7)).

To establish the validity of the formulation described above, we selected spherical and irregular powders for pure Ti and Ti-6Al-4V alloy, produced via atomization and milling respectively. The as-received atomized spherical pure Ti and Ti-6Al-4V alloy powders were manufactured by Advanced Powders and Coatings Inc., Quebec, Canada. The milled irregular pure Ti and Ti-6Al-4V alloy powders were prepared by ball milling of an elemental Ti powder (99.5 wt%) and a mixture of Ti (99.5 wt%), Al (99.8 wt%) and V (99.9 wt%) elemental powders at a rotational speed of 4.2 s^{-1} under a protection atmosphere of high purity argon in a high-energy planetary ball mill (QM-2SP20; apparatus factory of Nanjing University, Nanjing, China). The powder mixture was selected to correspond to the Ti-6Al-4V composition and was blended with stainless steel balls with diameters of 6, 10, and 15 mm respectively, the weight ratio of which was 1:3:1. The ball-to-powder mass ratios were approximately 7:1. The thermal behavior of the two family powders for pure Ti and Ti-6Al-4V alloy was measured under a high purity argon atmosphere with a heating rate of 20 °C/min by differential scanning calorimetry (DSC; Netzsch STA 409C, Bavaria, Germany). The morphology and particle size of the two types of powders for pure Ti and Ti-6Al-4V alloy were characterized using a Philips XL-30 FEG scanning electron microscope (SEM; Amsterdam, The Netherlands). Subsequently, the two types of powders for pure Ti and Ti-6Al-4V alloy were sintered under the protection of argon atmosphere using spark plasma sintering system (SPS-825, Sumitomo Coal Mining Co. Ltd., Japan). To minimize variations between the experiments, the same weight powder of 8 g used in both cases and was loaded into a graphite die with a 15 mm inner diameter. Additional details regarding SPS can be found in Refs [3–5]. Finally, to determine the values of f and Q for the two types of powders, the sintering parameters such as temperature (T), linear shrinkage (L) and time (t) were recorded via software.

Fig. 1 shows DSC curves of the atomized and milled powders for pure Ti and Ti-6Al-4V alloy, respectively. The atomized powders reveal spherical morphologies with sizes in the ranges of 15–53 and 15–45 μm for pure Ti and Ti-6Al-4V alloy, respectively. In contrast, morphologies of the milled powders are irregular, with sizes distribution in the ranges of 200–500 and 200–1000 μm for pure Ti and Ti-6Al-4V alloy, respectively. The smaller value of D corresponding to the atomized powders likely yields a higher γ compared to that of the milled powders. Moreover, it is well established that different crystalline defects have different relative contributions to raise the free energy of the metallic materials [14], and that the maximum energy contributed by grain size (1 nm) and disorder is 10 and 12 kJ/mol, respectively, far higher than that (1 kJ/mol) contributed by dislocations (10^{16}/m^2) or vacancies (1%). Therefore, the area of the exothermic peak in DSC curves likely corresponds to the release value of stored energy contributed by different crystalline defects [15,16]. By differentiating the DSC curve, the inflexion point at which the exothermic event starts and ends can be determined. The area of the exothermic peaks for the atomized and milled powders is calculated to be 653.4 and 1405.4 J/mol (Fig. 1), and 171.2 and 504.3 J/mol (Fig. 1 inset), respectively, for Ti-6Al-4V alloy and pure Ti, respectively. Reasonably, the larger area of the exothermic peaks or higher exothermic enthalpies indicate a higher concentration of crystalline defects in the milled powders. Accordingly, a smaller D, higher γ, and smaller exothermic enthalpies of the atomized powders will likely influence the densification mechanism relative to that of the milled counterparts.

On the basis of the variation in the height of the sintered compacts, an instantaneous relative density was calculated by Eq. (1). Fig. 2 shows the relative density of atomized and milled Ti-6Al-4V alloy powders as a function of temperature with various heating rates. The atomized powder has higher initial relative density of about 0.68 ± 0.01 compared to that of the milled counterpart (0.65 ± 0.01). This is attributed to the smaller D and more regular geometry of the atomized

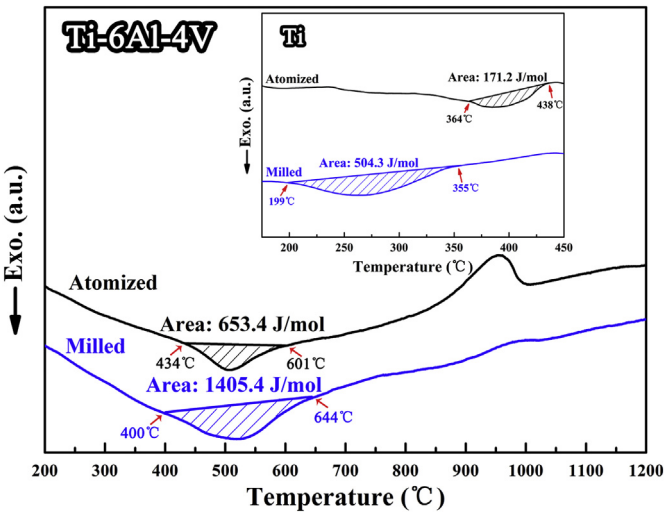

Fig. 1. DSC curves of the atomized and milled powders for Ti-6Al-4V alloy and pure Ti.

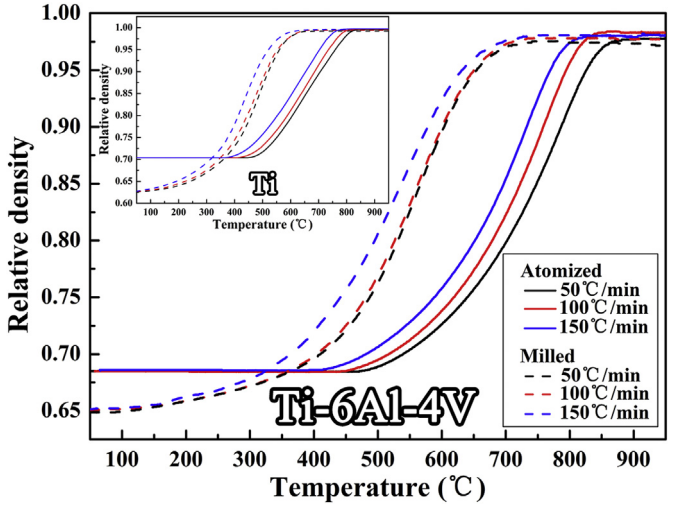

Fig. 2. Relative density of the atomized and milled powders as a function of temperature with various heating rates for Ti-6Al-4V alloy and pure Ti.

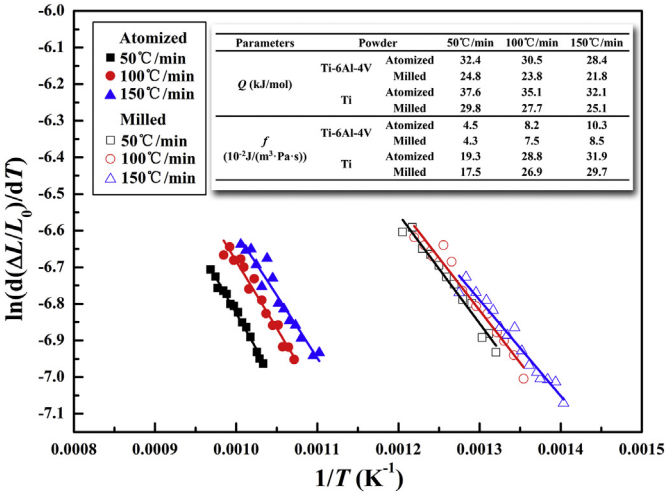

Parameters	Powder		50℃/min	100℃/min	150℃/min
Q (kJ/mol)	Ti-6Al-4V	Atomized	32.4	30.5	28.4
		Milled	24.8	23.8	21.8
	Ti	Atomized	37.6	35.1	32.1
		Milled	29.8	27.7	25.1
f (10^{-2}J/(m^3·Pa·s))	Ti-6Al-4V	Atomized	4.5	8.2	10.3
		Milled	4.3	7.5	8.5
	Ti	Atomized	19.3	28.8	31.9
		Milled	17.5	26.9	29.7

Fig. 4. Plots of $\ln(d(\Delta L / L_0) / dT)$ versus $1/T$ of the atomized and milled Ti-6Al-4V alloy powders with various heating rates. The inset lists the derived comprehensive impact factors f and activation energies for viscous flow Q of the atomized and milled powders for Ti-6Al-4V alloy and pure Ti.

powder. All curves show a typical "S" type of densification process. From the figure, one can observe two interesting trends. First, the relative density of the two types of powders increases with increasing heating rate. Second, the atomized powder has a higher (early densification stage) and lower (final densification stage) relative density than those of the milled powder. Similar phenomenon can be observed for the atomized and milled pure Ti powders (Fig. 2 inset).

To provide insight into these observations, Fig. 3 plots instantaneous densification rates of the atomized and milled powders for Ti-6Al-4V alloy (Fig. 3a) and pure Ti (Fig. 3b) as a function of temperature for various heating rates, according to Eq. (2). The resulting plots show two interesting findings. First, increasing the heating rate increases the instantaneous densification rate for both types of powders. Second, the atomized powders have a lower instantaneous densification rate than that of the milled counterparts throughout the entire densification process. Note that the onset position of fast shrinkage during the instantaneous densification rate for the milled powders always shifts to the left as compared to that of the atomized counterparts. This onset position approximately corresponds to the onset exothermic temperature in the DSC curves, as shown in Figs. 1 and 3. Accordingly, these results depend on the physical properties of the powders, and hence on the values for f and Q.

On the basis of the above derivation, from Eq. (3) to Eq. (8), we can determine the values for f and Q. Fig. 4 shows plots of $\ln(d(\Delta L / L_0) / dT)$ versus $1/T$ for the atomized and milled Ti-6Al-4V alloy powders under various heating rates. Correspondingly, the derived f and Q values for Ti-6Al-4V alloy and pure Ti are listed in Fig. 4 inset. The results show that for a given heating rate, the values of derived f and Q for the atomized powders are significantly higher than the corresponding ones of the milled powders. Moreover, the value of f increases with increasing hearing rate, whereas the opposite trend is the case for Q. As defined in Eq. (8), f increases with increasing γ as well as decreasing D and η_0. In contrast to the milled powders, the atomized powders have smaller D and thus higher γ. Published results suggest that milled Ti powder has a higher value of η_0 relative to that of atomized powder [9]. Hence, the calculated value of f for the atomized powders is always higher than that of the milled powders for a given heating rate (Fig. 4 inset). Reasonably, the higher Q value for the atomized powders is thought to be related to the defect concentration, as reflected by measured smaller exothermic enthalpies (Fig. 1). In terms of other trends, the higher the heating rate, the lower the viscosity [17,18], and thus the higher the f and the lower the Q (Fig. 4 inset). This Q dependence on heating rate is consistent with that of other crystalline and amorphous alloy powders [7–9].

To demonstrate the validity of the formulation described above, the upper part of Fig. 3a shows an example describing three densification stages of the milled Ti-6Al-4V alloy powder at 50 °C/min. Hence, on

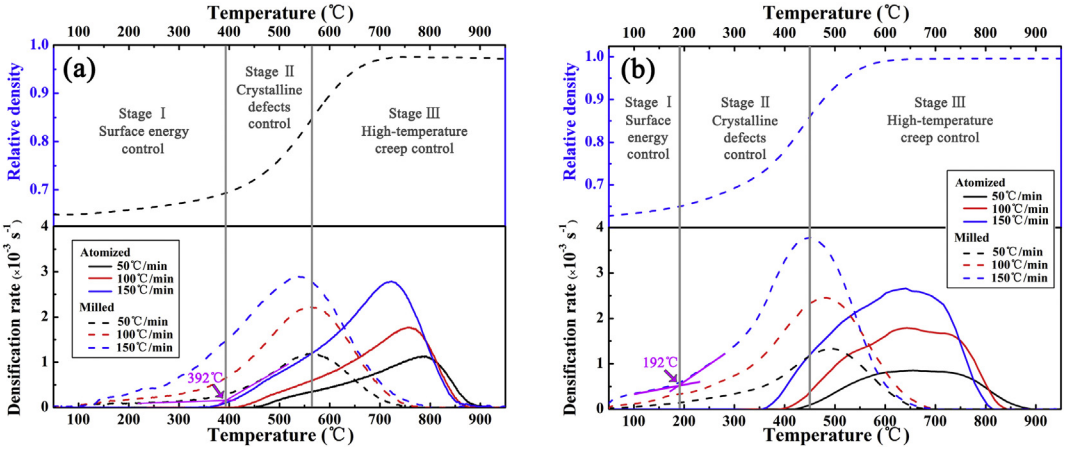

Fig. 3. Instantaneous densification rates (lower parts) of the atomized and milled powders as a function of temperature with various heating rates for Ti-6Al-4V alloy (a) and pure Ti (b). The upper parts show examples describing three densification stages of the milled Ti-6Al-4V alloy powder at 50 °C/min (a) and pure Ti powder (b) at 150 °C/min.

the basis of the values of the *f* and *Q*, we can assess specific densification stage of the atomized and milled Ti-6Al-4V alloy powders under a specific heating rate. Based on three different mechanisms, the densification of the two types of powders can be divided into three stages, i.e., surface energy control (stage I), crystalline defect control (stage II), and high-temperature creep control (stage III). In stage I below 392 °C, determined by the intersection point of the tangents of the instantaneous densification rate curve (the lower part of Fig. 3a), the densification is dominated mainly by surface energy, and thus the higher *f* of the atomized powder indicates the higher relative density compared to that of the milled powder (Figs. 2 and 4). It is important to note that there will be temperature variations caused by the 1.5 mm distance between the thermocouple and the edge of the powders during SPS; hence, the transition temperature of 392 °C (Fig. 3a), is in general agreement with the starting temperature of the exothermic peak, 400 °C (Fig. 1). In stage II ranging from 392 °C to 567 °C, the densification is dominated mainly by the free energy contributed by various crystalline defects; the higher the *Q* induced by the smaller exothermic enthalpy of the atomized powder (Fig. 1), the lower the relative density relative to the milled powder (Figs. 2 and 4). The transition temperature of 567 °C was determined as the maximum value of the instantaneous densification rate (the lower part of Fig. 3a). Finally, in stage III above 567 °C, the densification is dominated by high-temperature creep induced by fast growth of grains and subsequent softening of the metal powders. Undoubtedly, the validity of the formulation can be further authenticated by the similar three densification stages of the milled pure Ti powder at 150 °C/min, as shown in the upper part of Fig. 3b.

In summary, we described a formulation that can be used to provide insight into the densification mechanism that are active in atomized and milled powders for Ti-6Al-4V alloy and pure Ti, during spark plasma sintering. The values of *f* and *Q* can be used to assess the mechanism that controls each stage of densifications. Correspondingly, the higher *f* and *Q* for the atomized powders determine the higher and lower relative density compared to the milled counterparts, respectively.

Acknowledgement

This work was supported by the National Natural Science Foundation of China (No. 51574128), the Guangdong Natural Science Foundation for Research Team (No. 2015A030312003), the Guangdong Application-oriented Special Funds for Science and Technology R&D (No. 2016B090931002), and the Fundamental Research Funds for the Central Universities (No. 2017PY014). EJL and ZF would like to acknowledge ARO (Army Research Office: W911NF-16-1-0269) for financial support.

Appendix A. Supplementary data

Supplementary data to this article can be found online at http://dx.doi.org/10.1016/j.scriptamat.2017.06.034.

References

[1] Z.A. Munir, U. Anselmi-Tamburini, M. Ohyanagi, J. Mater. Sci. 41 (2006) 763–777.
[2] G. Xie, D.V. Louzguine-Luzgin, H. Kimura, A. Inoue, Appl. Phys. Lett. 90 (2007) 1–3.
[3] L.H. Liu, C. Yang, L.M. Kang, S.G. Qu, X.Q. Li, W.W. Zhang, W.P. Chen, Y.Y. Li, P.J. Li, L.C. Zhang, Sci Rep 6 (2016) 23467.
[4] L.H. Liu, C. Yang, F. Wang, S.G. Qu, X.Q. Li, W.W. Zhang, Y.Y. Li, L.C. Zhang, Mater. Des. 79 (2015) 1–5.
[5] L.H. Liu, C. Yang, L.M. Kang, Y. Long, Z.Y. Xiao, P.J. Li, L.C. Zhang, Mater. Sci. Eng. A 650 (2016) 171–182.
[6] S.J.L. Kang, Sintering, Elsevier Butterworth-Heinemann, Oxford, 2005.
[7] L.H. Liu, C. Yang, Y.G. Yao, F. Wang, W.W. Zhang, Y. Long, Y.Y. Li, Intermetallics 66 (2015) 1–7.
[8] T. Paul, S.P. Harimkar, Scr. Mater. 126 (2017) 37–40.
[9] V.V. Dabhade, T.R.R. Mohan, P. Ramakrishnan, Mater. Res. Bull. 42 (2007) 1262–1268.
[10] S. Diouf, A. Molinari, Powder Technol. 221 (2012) 220–227.
[11] Y. Han, J.L. Fan, T. Liu, H.C. Cheng, J.M. Tian, Int. J. Refract. Met. Hard Mater. 29 (2011) 743–750.
[12] J. Frenkel, J. Phys. 9 (1945) 385–391.
[13] Q. Chen, C.Y. Tang, K.C. Chan, L. Liu, J. Alloys Compd. 557 (2013) 98–101.
[14] S. Sharma, R. Vaidyanathan, C. Suryanarayana, Appl. Phys. Lett. 90 (2007) 111915.
[15] Y.H. Zhao, H.W. Sheng, K. Lu, Acta Mater. 49 (2001) 365–375.
[16] C. Yang, Z. Ding, J.A. Lin, S.G. Qu, X.Q. Li, W.W. Zhang, Y.Y. Li, Adv. Eng. Mater. 17 (2015) 1383–1390.
[17] E. Bakke, R. Busch, W.L. Johnson, Appl. Phys. Lett. 67 (1995) 3260–3262.
[18] T. Yamasaki, S. Maeda, Y. Yokoyama, D. Okai, T. Fukami, H.M. Kimura, A. Inoue, Intermetallics 14 (2006) 1102–1106.